Acta Oto-Laryngologica, 2010; 130: 95–100

informa
healthcare

ORIGINAL ARTICLE

Hydrogen protects vestibular hair cells from free radicals

AKIKO TAURA[1], YAYOI S KIKKAWA[2], TAKAYUKI NAKAGAWA[1] & JUICHI ITO[1]

[1]*Department of Otolaryngology-Head and Neck Surgery, Graduate School of Medicine, Kyoto University, Kyoto and* [2]*Department of Otolaryngology-Head and Neck Surgery, Graduate School of Medicine, University of Tokyo, Tokyo, Japan*

Abstract

Conclusion: Hydrogen gas effectively protected against the morphological and functional vestibular hair cell damage by reactive oxygen species (ROS). *Objective:* ROS are generally produced by oxidative stress. In the inner ear, ROS levels increase as a result of noise trauma and ototoxic drugs and induce damage. It is thus important to control ROS levels in the inner ear. The protective effects of hydrogen gas in cochlear hair cells have been reported previously. *Methods:* This study examined the effects of hydrogen gas on mouse vestibular hair cell damage by ROS using antimycin A. *Results:* In the group *exposed to hydrogen gas, vestibular hair cells were morphologically well preserved and their mechano-electrical transduction activities were relatively well maintained when compared with controls. Hydroxyphenyl fluorescein (HPF) fluorescence in vestibular tissue was also reduced by hydrogen gas.

Keywords: *Reactive oxygen species, vestibular hair cells, mechano-electrical transduction*

Introduction

Numerous patients suffer from balance disorders and the number increases with age. Vestibular hair cells also degenerate with age [1] and are damaged by oxidative stress [2]. Oxidative stress is one of the most important factors related to disorders of the inner ear [3–5]. In the inner ear, levels of reactive oxygen species (ROS) increase as a result of noise trauma and ototoxic drugs [6–10] and induce damage. It is thus important to control ROS levels in the inner ear.

Hydrogen molecules have recently been reported to act as an antioxidant that selectively reduces hydroxyl radicals, and have been shown to decrease cerebral infarction volume after ischemia [11]. Hydrogen gas also shows protective effects in hepatic injury [12], myocardial infarction [13], and glucose metabolism in patients with type 2 diabetes [14]. In the cochlea, Kikkawa et al. reported that hydrogen gas alleviated ROS-induced ototoxicity [15]. We thus applied their method to vestibular hair cells and investigated hair cell function. The function of hair cells was monitored by accumulation of FM1-43, which is known to reflect the activity of mechano-electrical transducer (MET) channels [16]. We also evaluated the generated hydroxyl radicals by fluorescence emission of 2-[6-(40-hydroxy) phenoxy-3H-xanthen-3-on-9-yl] benzoate (HPF) to examine the protective mechanisms.

Material and methods

Animals

ICR mice at 2 postnatal days (P2) were used in this study and were purchased from Shimizu Experimental Animals (Hamamatsu, Japan). The Animal Research Committee of the Kyoto University Graduate School of Medicine approved all experimental protocols.

Correspondence: Dr Akiko Taura, Department of Otolaryngology Head and Neck Surgery, Graduate School of Medicine, Kyoto University, Sakyo-ku, Kyoto 606-8507, Japan. E-mail: taura@ent.kuhp.kyoto-u.ac.jp

(Received 1 April 2010; accepted 11 April 2010)

ISSN 0001-6489 print/ISSN 1651-2251 online
DOI: 10.3109/00016489.2010.486799

Vestibular maculae explant culture

P2 ICR mice were deeply anesthetized with diethyl ether and decapitated. The temporal bones were dissected and the vestibular maculae were freed from the surrounding tissue and placed in 0.01 M phosphate-buffered saline (PBS; pH 7.4). After removing the otoconia, samples were placed on 12 mm collagen-coated cover glasses (4912-010, Iwaki, Asahi Glass Co. Ltd, Tokyo, Japan), followed by culture in serum-free modified Eagle's medium (MEM; Invitrogen, Eugene, OR, USA) supplemented with 3 g/l glucose (Wako Pure Chemicals, Osaka, Japan) and 0.3 g/l penicillin G (Wako), for 24 h at 37°C in humidified (95%) air:5% CO_2.

Antimycin A application and hydrogen treatment

Explants were incubated in medium containing antimycin A (Sigma-Aldrich, St Louis, MO, USA) at a final concentration of 1 μg/ml. Cultures were maintained for 24 h. At the same time, explants were cultured initially in an airtight box (Chopla Industries, Inazawa, Japan) with reduced CO_2-dependence media, MEM, and Leivovitz's L-15 medium (Invitrogen, CA, USA) mixed in a 1:1 ratio [14], supplemented with 3 g/l glucose and 0.3 g/l penicillin G, at 37°C in humidified (100%) atmospheric air. After 24 h, the medium was changed to one containing antimycin A at a concentration of 1 μg/ml, with or without hydrogen gas for another 24 h. Hydrogen gas was dissolved directly into the media, and a high content of dissolved hydrogen (1.3 ± 0.1 mg/l) was confirmed using a hydrogen electrode (Model M-10B2; Able Corporation, Tokyo, Japan). The pH of the culture media without hydrogen gas was 7.18 ± 0.02, and that of culture media with hydrogen gas was 7.52 ± 0.02. The prepared media were used for culture within 30 min.

Immunohistological analysis

At the end of the culture period, samples were fixed for 15 min in 4% paraformaldehyde in 0.1 M phosphate buffer (pH 7.4), and then provided for immunostaining for myosin VIIa to evaluate the number of surviving hair cells. Specimens were incubated with primary rabbit polyclonal antibodies against myosin VIIa (1:500; Proteus Bioscience Inc., Ramona, CA, USA). Alexa-Fluor 568 goat anti-rabbit IgG (1:100; Invitrogen, CA, USA) was used as the secondary antibody. Specimens were then incubated in Alexa-Fluor 488-conjugated phalloidin (1:100; Invitrogen) to label F-actin. Specimens were examined with a Leica TCS-SP2 laser-scanning confocal microscope (Leica Microsystems Inc., Wetzlar, Germany). To quantify hair cell loss after treatments, hair cells were counted in more than three regions of vestibular epithelia.

Counting of remaining hair bundles

Remaining hair bundles were measured using a 10 × 40 eyepiece reticule. Each square of the reticule was 100 μm on each side. Remaining hair bundles were counted in each of three randomly selected fields containing both striolar and extrastriolar regions, and the values obtained were averaged. At least 10 vestibules were examined for each set of conditions.

FM1-43 accumulation of hair cells

A lipophilic dye, FM1-43 FX (Invitrogen), which has been shown to enter hair cells through transducer channels [16], was used to detect hair cells with active transducer channels by accumulation of FM1-43FX (5 μM FM1-43 in PBS, prepared from 10 mM stock solution in DMSO). The mechano-electrical transduction activity of hair cells was quantified based on dye accumulation by applying mechanical stimulation for 10 s [16]. Subsequently, explants were washed three times with PBS for 10 min each, followed by fixing with 4% PFA. FM1-43 accumulation within the cells was observed under a fluorescence microscope.

HPF analysis

At the end of the experiments, explants were treated with 30 mM HPF (Daiichi Pure Chemicals Co., Tokyo, Japan) for 20 min to detect cellular hydroxyl radicals.

Fluorescent images were captured with a Leica TCS-SP2 confocal microscope. All images were taken under the same laser intensity, detector gain, and offset values.

Statistical analysis

Quantitative differences were evaluated by two-way factorial analysis of variance (ANOVA). Significance was evaluated at a level of $p < 0.05$. Data are presented as means and standard errors, along with the number of explants under each condition.

Results

Protective effects of hydrogen gas on morphology

The effects of hydrogen gas on the vestibule are illustrated in Figure 1. In the absence of hydrogen gas, most hair bundles were eliminated and the number of myosin VIIa-positive cells was small (Figure 1A and C). However, in explants treated simultaneously with hydrogen gas, hair bundles tended to be preserved and numerous myosin VIIa-positive cells were observed (Figure 1B and D). The morphology of hair bundles without hydrogen gas was

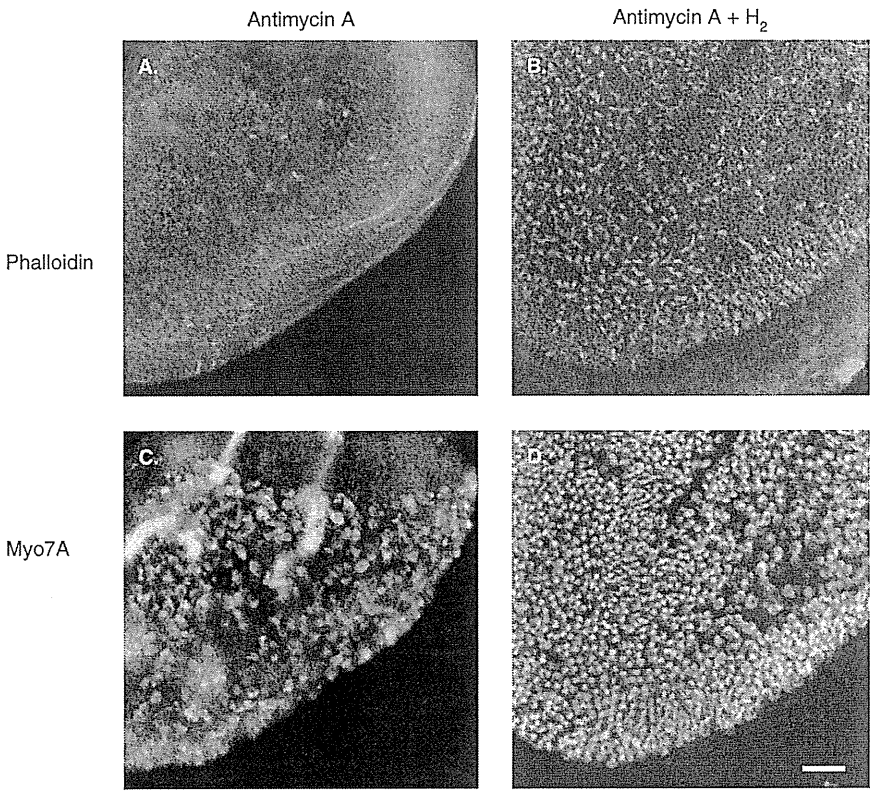

Figure 1. Effects of hydrogen gas in the vestibule. In the absence of hydrogen gas, most hair bundles were eliminated and the number of myosin VIIa-positive cells was small (A and C). However, in explants treated simultaneously with hydrogen gas, hair bundles were preserved and numerous myosin VIIa-positive cells were observed (B and D). Scale bar: 50 μm.

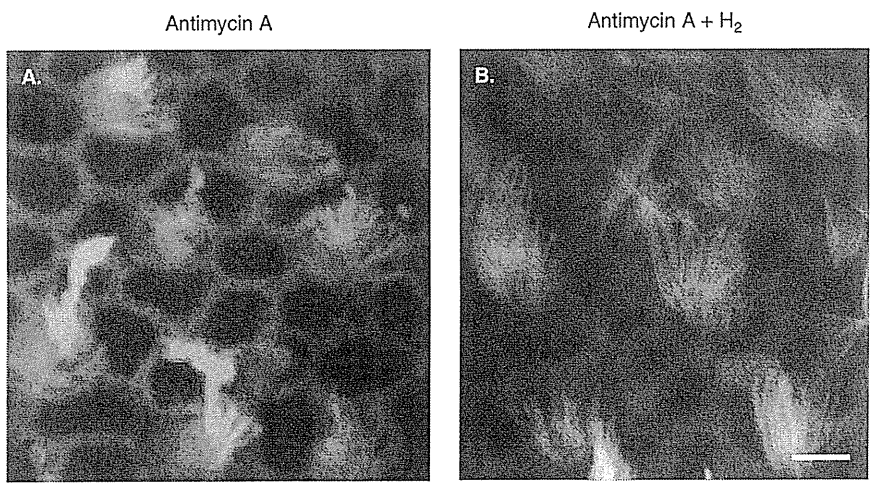

Figure 2. Morphology of hair bundles. The hair bundle without hydrogen gas was severely damaged (A). Some of them fused with each stereocilia or were fanned out. In contrast, the morphology of each hair bundle was preserved intact in the presence of hydrogen gas (B). Scale bar: 10 μm.

severely disrupted (Figure 2A). Some bundles showed fused or fanned out stereocilia. In contrast, the morphology of hair bundles was preserved in the presence of hydrogen gas (Figure 2B). The number of remaining hair bundles in the groups treated with hydrogen gas was significantly larger when compared with the group treated with antimycin A alone ($p < 0.05$; $n = 19$) (Figure 3).

Protective effects of hydrogen gas on function

The effects of hydrogen gas on vestibular hair cell function are illustrated in Figure 4.

In the absence of hydrogen gas, some hair cells showed FM1-43 accumulation (Figure 4A). However, in explants treated simultaneously with hydrogen gas, numerous hair cells showed FM1-43

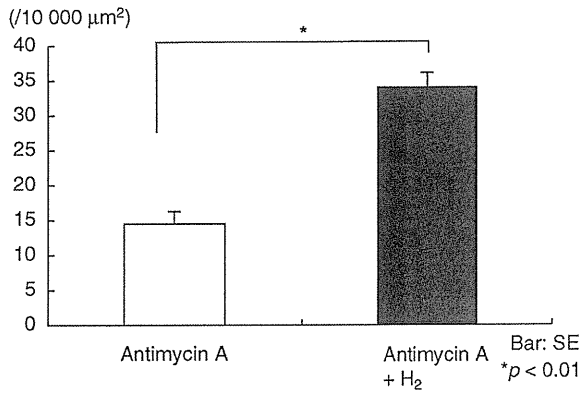

Figure 3. Number of remaining hair bundles. In the groups treated with hydrogen gas, the number of remaining hair bundles was significantly larger when compared with the group treated with antimycin A alone ($p < 0.05$; $n = 19$).

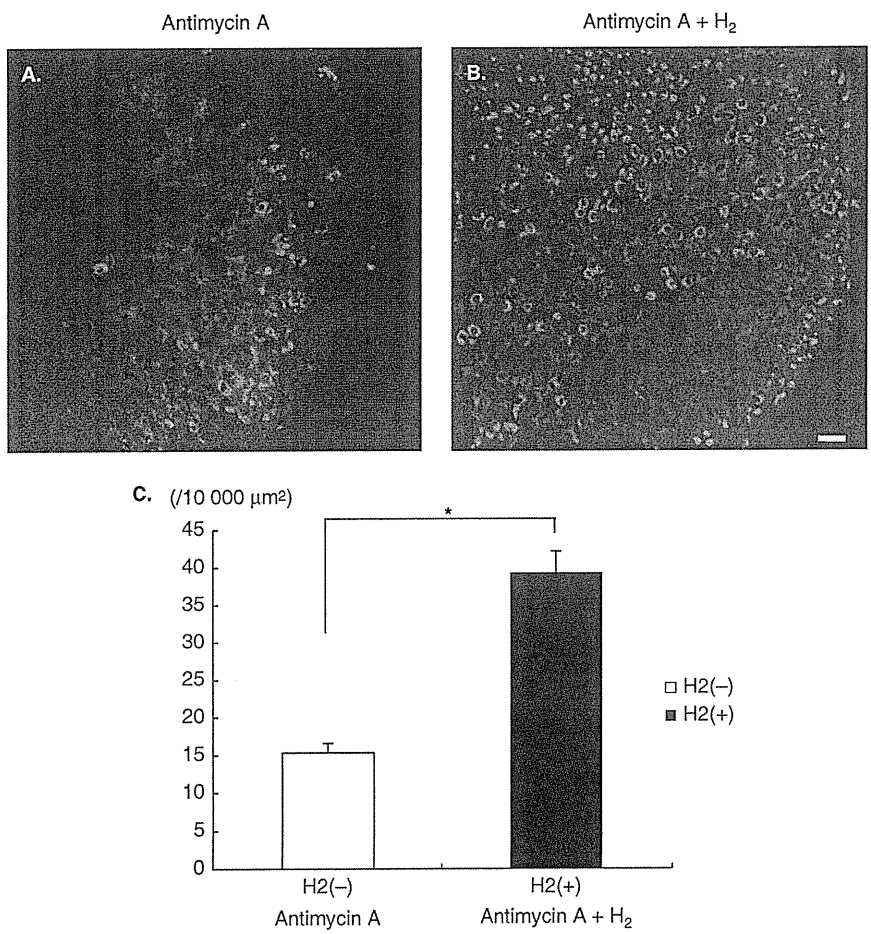

Figure 4. Effects of hydrogen gas on the function of vestibular hair cells. In the absence of hydrogen gas, few hair cells showed FM1-43-accumulation (A). However, in explants treated simultaneously with hydrogen gas, numerous hair cells showed FM1-43 accumulation. Scale bar: 20 μm (B). The number of FM1-43-positive hair cells in the group treated with hydrogen gas was significantly larger when compared with the group treated with antimycin A alone (*$p < 0.0001$; $n = 12$); bar: SE (C).

accumulation (Figure 4B). The number of FM1-43-positive hair cells in the groups treated with hydrogen gas was significantly larger when compared with the group treated with antimycin A alone ($p < 0.0001$; $n = 12$) (Figure 4C).

ROS reduction by hydrogen gas

To investigate the mechanisms of protection, we measured ROS production in explants (Figure 5). HPF is a reagent that was developed to directly detect certain ROS [17]. There were numerous HPF-positive cells after treatment with antimycin A (Figure 5A). In contrast, there were few HPF-positive cells in the group treated with hydrogen gas (Figure 5B). The number of HPF-positive hair cells in the group treated with hydrogen gas was significantly smaller when compared with the group treated with antimycin A alone ($p < 0.0001$; $n = 10$) (Figure 5C).

Discussion

Kikkawa et al. [15] previously reported the effects of hydrogen gas on cochlear hair cells against ROS toxicity with antimycin A. In this study, we used the same method and applied it to vestibular hair cells. Initially, we used three different antimycin A concentrations, and we found that 10 μg/ml resulted in severe damage and 0.01 μg/ml resulted in insufficient damage (data not shown). Our results showed that hydrogen gas has protective effects on vestibular hair cells against ROS toxicity by reducing the production of ROS.

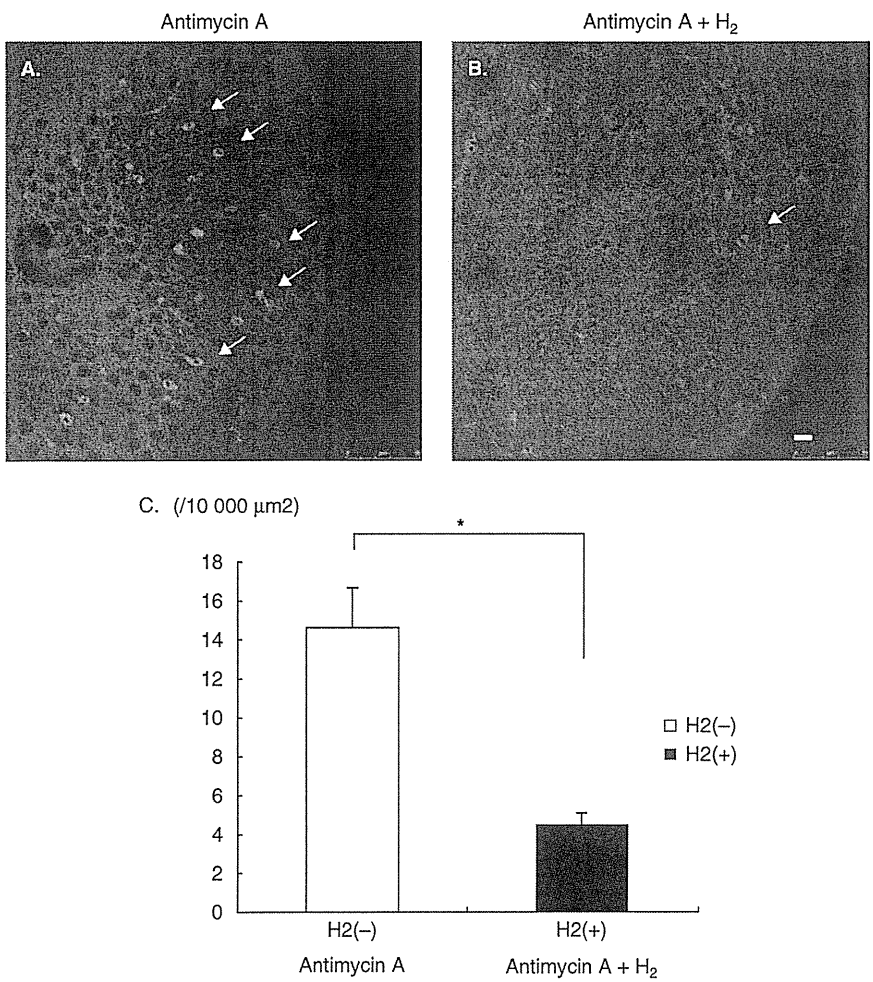

Figure 5. HPF analysis. There were numerous HPF-positive cells after treatment with antimycin A in the absence of hydrogen gas (A). In contrast, there were a few HPF-positive cells in the group treated with hydrogen gas (B). The number of HPF-positive hair cells in the group treated with hydrogen gas was significantly smaller when compared with the group treated with antimycin A alone (bar: SE; *$p < 0.0001$; $n = 10$) (C).

There are two hypotheses regarding the mechanisms by which ROS induce cell damage; ROS may induce activation of caspase-3, which causes apoptosis [18], or ROS may induce increases in calcium concentration, thus leading to necrosis [19]. In our experiment, activation of caspase-3 was observed in the group treated with antimycin A alone (data not shown). Thus, it is possible that hydrogen gas reduces the production of ROS and prevents the activation of caspase-3, thus preventing apoptosis.

Ohsawa et al. [11] demonstrated that hydrogen gas has some unique properties. Hydrogen gas can permeate the blood–brain barrier, which is very important in the inner ear, as it is difficult for medicines to reach hair cells because of this barrier [20,21]. Hydrogen gas also has specific activity against detrimental ROS, such as the hydroxyl radical and peroxynitrite, while the metabolic oxidation-reduction reaction and other less potent ROS are not affected. Therefore, hydrogen gas may be a promising treatment for balance disorders. However, further basic and clinical investigations are required.

Conclusion

In conclusion, we showed that hydrogen gas markedly decreases oxidative stress by scavenging ROS, thus protecting vestibular hair cells against oxidative stress. These results have prompted us to perform in vivo studies to determine whether treatment with hydrogen gas exerts beneficial effects on damaged vestibules to ameliorate balance disorders.

Acknowledgments

This study was supported by a Health and Labor Science Research Grant for Research on Specific Disease (Vestibular Disorders) from the Ministry of Health, Labor and Welfare, Japan (2009).

Declaration of interest: The authors report no conflicts of interest. The authors alone are responsible for the content and writing of the paper.

References

[1] Walther LE, Westhofen M. Presbyvertigo-aging of otoconia and vestibular sensory cells. J Vestib Res 2007;17:89–92.

[2] Tanigawa T, Tanaka H, Hayashi K, Nakayama M, Iwasaki S, Banno S, et al. Effect of hydrogen peroxide on vestibular hair cells in the guinea pig: importance of cell membrane impairment preceding cell death. Acta Otolaryngol 2008;128:1196–202.

[3] Maetani T, Hakuba N, Taniguchi M, Hyodo J, Shimizu Y, Gyo K. Free radical scavenger protects against inner hair cell loss after cochlear ischemia. Neuroreport 2003;14:1881–4.

[4] Staecker H, Zheng QY, Van De Water TR. Oxidative stress in aging in the C57B16/J mouse cochlea. Acta Otolaryngol 2001;121:666–72.

[5] Yamasoba T, Schacht J, Shoji F, Miller JM. Attenuation of cochlear damage from noise trauma by an iron chelator, a free radical scavenger and glial cell line-derived neurotrophic factor in vivo. Brain Res 1999;815:317–25.

[6] Seidman MD, Shivapuja BG, Quirk WS. The protective effects of allopurinol and superoxide dismutase on noise-induced cochlear damage. Otolaryngol Head Neck Surg 1993;109:1052–6.

[7] Otto WC, Brown RD, Gage-White L, Kupetz S, Anniko M, Penny JE, et al. Effects of cisplatin and thiosulfate upon auditory brainstem responses of guinea pigs. Hear Res 1988;35:79–85.

[8] Takumida M, Anniko M, Popa R, Zhang DM. Pharmacological models for inner ear therapy with emphasis on nitric oxide. Acta Otolaryngol 2001;121:16–20.

[9] Yamane H, Nakai Y, Takayama M, Iguchi H, Nakagawa T, Kojima A. Appearance of free radicals in the guinea pig inner ear after noise-induced acoustic trauma. Eur Arch Otorhinolaryngol 1995;252:504–8.

[10] Yamashita D, Jiang HY, Schacht J, Miller JM. Delayed production of free radicals following noise exposure. Brain Res 2004;1019:201–9.

[11] Ohsawa I, Ishikawa M, Takahashi K, Watanabe M, Nishimaki K, Yamagata K, et al. Hydrogen acts as a therapeutic antioxidant by selectively reducing cytotoxic oxygen radicals. Nat Med 2007;13:688–94.

[12] Fukuda K, Asoh S, Ishikawa M, Yamamoto Y, Ohsawa I, Ohta S. Inhalation of hydrogen gas suppresses hepatic injury caused by ischemia/reperfusion through reducing oxidative stress. Biochem Biophys Res Commun 2007;361:670–4.

[13] Hayashida K, Sano M, Ohsawa I, Shinmura K, Tamaki K, Kimura K, et al. Inhalation of hydrogen gas reduces infarct size in the rat model of myocardial ischemia-reperfusion injury. Biochem Biophys Res Commun 2008;373:30–5.

[14] Kajiyama S, Hasegawa G, Asano M, Hosoda H, Fukui M, Nakamura N, et al. Supplementation of hydrogen-rich water improves lipid and glucose metabolism in patients with type 2 diabetes or impaired glucose tolerance. Nutr Res 2008;28:137–43.

[15] Kikkawa YS, Nakagawa T, Horie RT, Ito J. Hydrogen protects auditory hair cells from free radicals. Neuroreport 2009;20:689–94.

[16] Gale JE, Marcotti W, Kennedy HJ, Kros CJ, Richardson GP. FM1–43 dye behaves as a permeant blocker of the hair cell mechanotransducer channel. J Neurosci 2001;21:7013–25.

[17] Setsukinai K, Urano Y, Kakinuma K, Majima HJ, Nagano T. Development of novel fluorescence probes that can reliably detect reactive oxygen species and distinguish specific species. J Biol Chem 2003;278:3170–5.

[18] Labbé D, Teranishi MA, Hess A, Bloch W, Michel O. Activation of caspase-3 is associated with oxidative stress in the hydropic guinea pig cochlea. Hear Res 2005;202: 21–7.

[19] Horner KC, Guilhaume A. Ultrastructural changes in the hydropic cochlea of the guinea-pig. Eur J Neurosci 1995;7: 1305–12.

[20] Coimbra RS, Loquet G, Leib SL. Limited efficacy of adjuvant therapy with dexamethasone in preventing hearing loss due to experimental pneumococcal meningitis in the infant rat. Pediatr Res 2007;62:291–4.

[21] Laurell GF, Teixeira M, Duan M, Sterkers O, Ferrary E. Intact blood-perilymph barrier in the rat after impulse noise trauma. Acta Otolaryngol 2008;128:608–12.

Direct and instantaneous observation of intravenously injected substances using intravital confocal micro-videography

Yu Matsumoto,[1,2,3] Takahiro Nomoto,[4] Horacio Cabral,[4] Yoko Matsumoto,[5] Sumiyo Watanabe,[1,6,7] R. James Christie,[8] Kanjiro Miyata,[1] Makoto Oba,[9] Tadayoshi Ogura,[10] Yuichi Yamasaki,[8] Nobuhiro Nishiyama,[1] Tatsuya Yamasoba,[2] and Kazunori Kataoka[1,4,8,*]

[1]*Division of Clinical Biotechnology, Center for Disease Biology and Integrative Medicine, Graduate School of Medicine, The University of Tokyo, Japan*
[2]*Department of Otorhinolaryngology and Head and Neck Surgery, Graduate School of Medicine and Faculty of Medicine, The University of Tokyo, Japan*
[3]*Department of Otorhinolaryngology and Head and Neck Surgery, Mitsui Memorial Hospital, Japan*
[4]*Department of Bioengineering, Graduate School of Engineering, The University of Tokyo, Japan*
[5]*Department of Obstetrics and Gynecology, Graduate School of Medicine and Faculty of Medicine, The University of Tokyo, Japan*
[6]*Division of Nephrology and Endocrinology, Department of Internal Medicine, Graduate School of Medicine and Faculty of Medicine, The University of Tokyo, Japan*
[7]*Department of Internal Medicine, Teikyo University School of Medicine, Japan*
[8]*Department of Materials Engineering, Graduate School of Engineering, The University of Tokyo, Japan*
[9]*Department of Vascular Regeneration, Division of Tissue Engineering, The University of Tokyo Hospital, Japan*
[10]*Nikon Instech Co., Ltd., Japan*
**kataoka@bmw.t.u-tokyo.ac.jp*

Abstract: We describe the development and application of intravital confocal micro-videography to visualize entrance, distribution, and clearance of drugs within various tissues and organs. We use a Nikon A1R confocal laser scanning microscope system attached to an upright ECLIPSE FN1. The Nikon A1R allows simultaneous four channel acquisition and speed of 30 frames per second while maintaining high resolution of 512 × 512 scanned points. The key techniques of our intravital imaging are (1) to present a flat and perpendicular surface to the objective lens, and (2) to expose the subject with little or no bleeding to facilitate optical access to multiple tissues and organs, and (3) to isolate the subject from the body movement without compressing the blood vessels, and (4) to insert a tail vein catheter for timed injection without moving the subject. Ear lobe dermis tissue was accessible without surgery. Liver, kidney, and subcutaneous tumor were accessed following exteriorization through skin incision. In order to image initial extravasations of compounds into tissue following intravenous injection, movie acquisition was initialized prior to drug administration. Our technique can serve as a powerful tool for investigating biological mechanisms and functions of intravenously injected drugs, with both spatial and temporal resolution.

OCIS codes: (170.1790) Confocal microscopy; (170.2655) Functional monitoring and imaging.

References and links

1. I. Veilleux, J. A. Spencer, D. P. Biss, D. Cote, and C. P. Lin, "In Vivo Cell Tracking With Video Rate Multimodality Laser Scanning Microscopy," IEEE J. Sel. Top. Quantum Electron. 14(1), 10–18 (2008).
2. P. Kim, M. Puoris'haag, D. Côté, C. P. Lin, and S. H. Yun, "In vivo confocal and multiphoton microendoscopy," J. Biomed. Opt. 13(1), 010501 (2008).
3. P. Kim, E. Chung, H. Yamashita, K. E. Hung, A. Mizoguchi, R. Kucherlapati, D. Fukumura, R. K. Jain, and S. H. Yun, "In vivo wide-area cellular imaging by side-view endomicroscopy," Nat. Methods 7(4), 303–305 (2010).
4. R. Mehvar, M. A. Robinson, and J. M. Reynolds, "Molecular weight dependent tissue accumulation of dextrans: in vivo studies in rats," J. Pharm. Sci. 83(10), 1495–1499 (1994).

#135496 - $15.00 USD Received 27 Sep 2010; revised 16 Oct 2010; accepted 17 Oct 2010; published 21 Oct 2010

5. R. Mehvar, and T. L. Shepard, "Molecular-weight-dependent pharmacokinetics of fluorescein-labeled dextrans in rats," J. Pharm. Sci. 81(9), 908–912 (1992).
6. G. Zhang, V. Budker, and J. A. Wolff, "High levels of foreign gene expression in hepatocytes after tail vein injections of naked plasmid DNA," Hum. Gene Ther. 10(10), 1735–1737 (1999).
7. F. Liu, Y. Song, and D. Liu, "Hydrodynamics-based transfection in animals by systemic administration of plasmid DNA," Gene Ther. 6(7), 1258–1266 (1999).
8. H. Herweijer, and J. A. Wolff, "Progress and prospects: naked DNA gene transfer and therapy," Gene Ther. 10(6), 453–458 (2003).
9. D. Liu, and J. E. Knapp, "Hydrodynamics-based gene delivery," Curr. Opin. Mol. Ther. 3(2), 192–197 (2001).
10. A. Crespo, A. Peydró, F. Dasí, M. Benet, J. J. Calvete, F. Revert, and S. F. Aliño, "Hydrodynamic liver gene transfer mechanism involves transient sinusoidal blood stasis and massive hepatocyte endocytic vesicles," Gene Ther. 12(11), 927–935 (2005).
11. T. Suda, X. Gao, D. B. Stolz, and D. Liu, "Structural impact of hydrodynamic injection on mouse liver," Gene Ther. 14(2), 129–137 (2007).
12. G. Zhang, X. Gao, Y. K. Song, R. Vollmer, D. B. Stolz, J. Z. Gasiorowski, D. A. Dean, and D. Liu, "Hydroporation as the mechanism of hydrodynamic delivery," Gene Ther. 11(8), 675–682 (2004).
13. Y. Ohno, H. Birn, and E. I. Christensen, "In vivo confocal laser scanning microscopy and micropuncture in intact rat," Nephron, Exp. Nephrol. 99(1), e17–e25 (2005).

Introduction

In vivo imaging has received much attention in recent years, as it can elucidate the complex biological and pathological events within a living animal. Although histological examination of excised tissues has long served as a fundamental approach for tissue analysis, intravital confocal microscopy provides instant histopathology at the cellular and subcellular level and therefore is ideal for investigating dynamic events involved. Here we describe the development and application of intravital confocal micro-videography to visualize entrance, distribution, and clearance of drugs within various tissues and organs. In order to image initial extravasations of compounds into tissue following intravenous injection, movie acquisition was initialized prior to drug administration. Many groups have adapted commercial confocal microscopes for intravital imaging, but they often use conventional galvano scanners with slow acquisition speed. Progressive groups build confocal and/or multi-photon microscopes and even microendoscopes with rapid scanning systema in-house to achieve video-rate imaging [1–3].

Table 1. Commercially available rapid scanning confocal microscopes

Vendor	Product Name	Scanning System	Maximum Frame Rate at 512 x 512 Pixels	Number of Simultaneously Detectable Channels
Nikon	A1R	Resonant Scanner	30 fps	4
Leica Microsystems	TCS SP5 II	Resonant Scanner	25 fps	5
Carl Zeiss	LSM 7 LIVE	Linear Scanner	120 fps	2
Yokogawa Electric	CSU-X1	Nipkow spinning disk	2000 fps	3
Olympus	DSU	Spinning Disk Confocal	15 fps	1

Recently, several rapid scanning confocal microscopes became commercially available (Table 1). Although all vendors primarily recommend use of their products with an inverted configuration (optimized for live cell imaging), combination with an upright microscope has advantages for intravital imaging. Here, we attached a Nikon A1R confocal laser scanning microscope system to an upright ECLIPSE FN1 to acquire video images. The A1R incorporates both a conventional galvano scanner and also a high-speed resonant scanner, which allows an acquisition speed of 30 frames per second and simultaneous four channel detection, while maintaining high resolution of 512 × 512 scanned points.Our technique consists of the following essential features:

(1) Front-end design presenting a flat and perpendicular surface against the objective lens;

#135496 - $15.00 USD Received 27 Sep 2010; revised 16 Oct 2010; accepted 17 Oct 2010; published 21 Oct 2010

(2) Exposure surgery with little or no bleeding to facilitate optical access to multiple tissues and organs;

(3) Stabilization of the sample to isolate from the body movement without compressing the blood vessels;

(4) Tail vein catheterization for timed injection during data acquisition, without moving the subject;

Our technique is particularly effective for investigating the dynamic and complex events that occur immediately following drug administration. We investigated the influence of molecular weight on pharmacokinetic behavior by imaging the ear lobe dermis. We also investigated the accumulation of pDNA within liver tissue by hydrodynamic injection. Kidney and tumor tissues were imaged to observe renal excretion and tumor extravasation.

Results and discussion

During the development of a promising drug delivery system, there is a strong need to accurately grasp the intravital behavior of the administered drugs [4,5]. We investigated the influence of molecular weight on pharmacokinetic behavior using fluorescein (MW = 332) and fluorescein-labeled dextrans (FD) with average molecular weights of 10-, 40-, and 500 kDa (Fig. 1). Fluorescein and FDs demonstrated different pharmacokinetics [Fig. 1(c), 1(e), Media 1, Media 2, Media 3, and Media 4]. Arterial entrance was observed 10 seconds after injection, followed by venous migration 30 seconds after injection. Fluorescein diffused into extravascular tissue concurrently with venous migration. FD 10 kDa gradually translocated into extravasculature tissue 10-15 minutes after injection and lymphatic drainage was observed after 20 minutes. FD 70- and 500 kDa remained in the vasculature during the entire 60-minute observation period. Our confocal micro-videography technique is superior to conventional methods used to study plasma clearance in regard to the number of animals needed to generate a clearance curve and also the ability to obtain more information from a single experiment. Conventional protocols used in plasma clearance studies require blood extraction at various post-injection time points, using multiple animals. In contrast, intravital confocal micro-videography yields 30 time points per seconds before, during, and after the injection. Moreover, our technique provides spatial resolution so that we can individually investigate multiple regions such as arteries, veins, extravascular tissue, lymphatic vessels, and even cells and nuclei if desirable [Fig. 1(d)]. For long-term plasma clearance studies, however, we still perform conventional methods in conjunction with our technique because prolonged anesthesia periods longer than five hours are not practical.

#135496 - $15.00 USD Received 27 Sep 2010; revised 16 Oct 2010; accepted 17 Oct 2010; published 21 Oct 2010

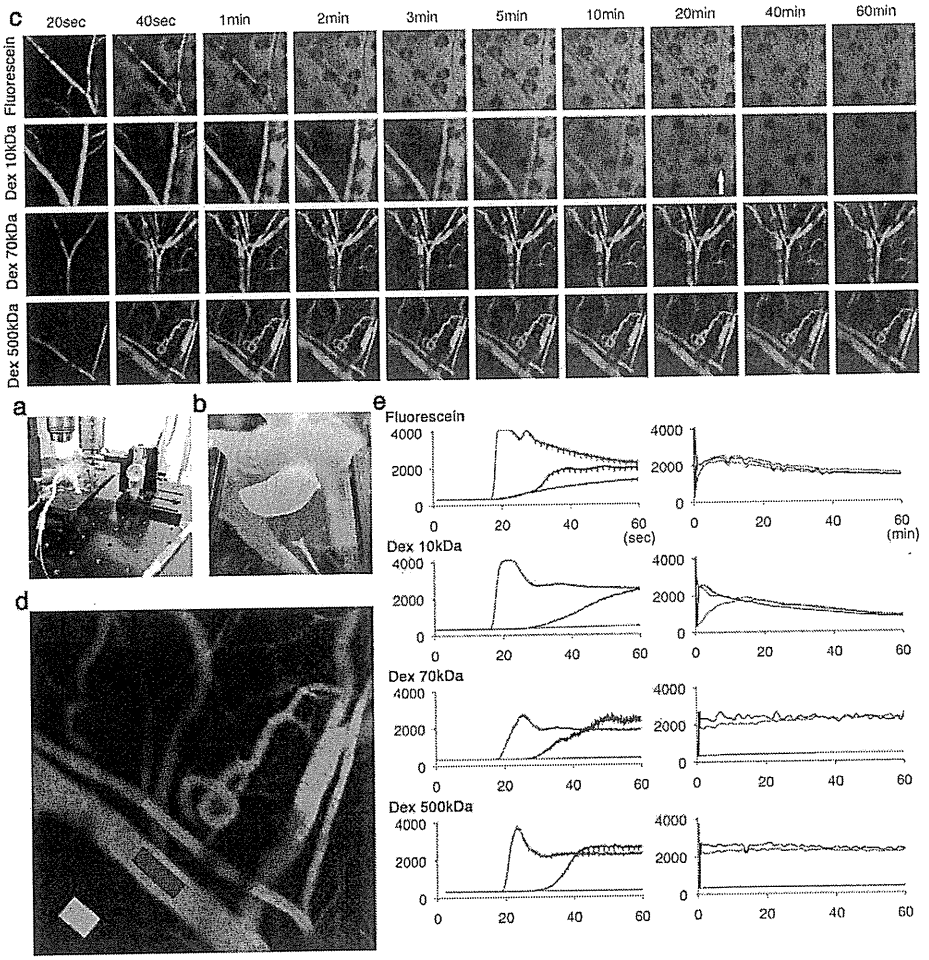

Fig. 1. (a) The earlobe is an excellent location for intravital confocal micro-videography because blood vessels are easily observed in the dermis and the ear is easily accessed and positioned in the imaging apparatus. (b) Earlobe was attached to the coverslip with a small drop of immersion oil. (c) Fluorescein, FD 10-, 70-, and 500 kDa were administered via tail vein catheter 10 seconds after movie acquisition was initiated. Video-rate (30 fps) movies were recorded for the first minute, and subsequent time-lapse images were recorded every minute for an additional 60 minutes. The arrow indicates lymphatic drainage. Obtained data sets were further processed using Nikon NIS-Elements C software. Image size: 645.50μm x 645.50μm. (d) Three regions of interest (ROI) are selected respectively as an artery (red), vein (blue), and extravascular skin tissue (green). Image size: 645.50μm x 645.50μm. (e) Fluorescence intensity in these ROIs plotted against time. All movies are provided as supplementary movie files (Media 1, Media 2, Media 3, and Media 4).

The liver is a vital organ that has a wide range of functions, including detoxification, protein synthesis, storage, and production of bile. Real-time imaging of liver dynamics and small changes in hepatocytes will provide insight to poorly understood processes that occur in the liver. We applied our real-time imaging technique to observe the accumulation of pDNA within liver tissue by hydrodynamic injection [Fig. 2(a)]. Delivery of pDNA by hydrodynamic injection involves rapid tail vein injection of a large volume of pDNA solution and efficient accumulation of pDNA in the liver is reported [6,7]. This method has been widely utilized by the gene therapy community for evaluating therapeutic activities of various genes [8,9].

#135496 - $15.00 USD Received 27 Sep 2010; revised 16 Oct 2010; accepted 17 Oct 2010; published 21 Oct 2010

Following normal injection, pDNA flowed into the hepatic lobule from the hepatic artery, through the sinusoids, and towards the central vein (Media 5). After 20 minutes, pDNA was observed adjacent to vessel walls, but was rarely transferred into hepatic cells. In contrast, hydrodynamic injection of pDNA resulted in initial flow into the hepatic lobule from the hepatic artery, but the flow stopped at the sinusoids. After 50 seconds, pDNA appeared from the central vein, indicating retrodynamic blood flow. Blood flow oscillated back and forth within the sinusoids, indicating that the blood pressure of central and portal vein remained in equilibrium, which lasted as long as 3 minutes (Media 6). During the 30-minute period after injection, pDNA was observed in more hepatic cell nuclei by hydrodynamic injection than normal injection. It has been hypothesized that hydrodynamic injection generates retrodynamic blood flow from the central vein [10–12]. This hypothesis was well described by performing dual pressure detector system of the portal vein and inferior vena cava, and is further supported by our results obtained by direct imaging of the hepatic lobule.

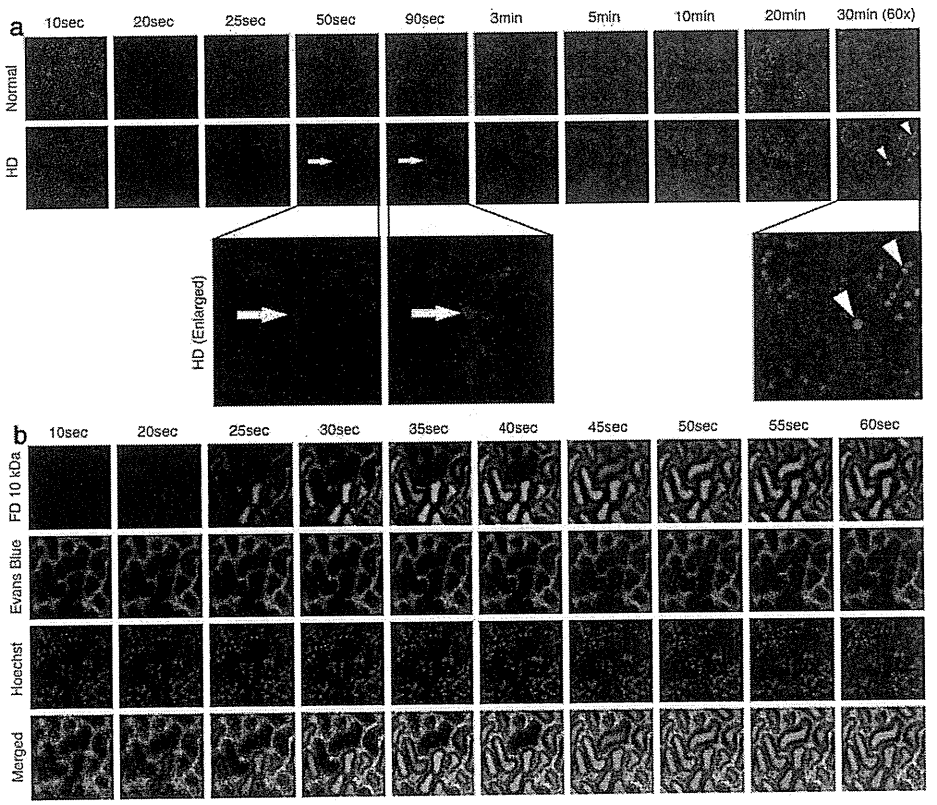

Fig. 2. (a) Intravital confocal micro-videography of the mouse hepatic lobule. Hoechst (blue) was intravenously injected 15 minutes before imaging. Cy5-labeled pDNA (red) were normally or hydrodynamically (HD) injected via tail vein catheter 10 seconds after movie acquisition was initiated (Media 5 and Media 6). Image frames were extracted from both videos at identical time points for comparison. Image size: 645.50μm x 645.50μm. Zoomed pictures were taken 30 minutes after injection. Image size: 212.13μm x 212.13μm. Hoechst channels are shown at 10 sec and 30 min for histological comprehension. Arrows indicate reverse blood flow from central vein. Arrowheads indicate nuclei that pDNA were successfully transferred. (b) Intravital confocal micro-videography of mouse kidney tissue. Hoechst (blue) and Evan's Blue dye (red) were intravenously injected 15 minutes and 5 minutes before imaging, respectively. FD 10 kDa (green) were administered via tail vein catheter 10 seconds after movie acquisition was initiated (Media 7). Image size: 645.50μm x 645.50μm.

#135496 - $15.00 USD Received 27 Sep 2010; revised 16 Oct 2010; accepted 17 Oct 2010; published 21 Oct 2010

To further demonstrate the feasibility of our technique, kidney and tumor tissues were imaged to observe renal excretion and tumor extravasation. Deeper kidney structures such as glomeruli could not be imaged because renal tissue highly absorbs and scatters light [13]. Although the imaging of the renal cortex was limited to shallow features such as proximal and distal tubules and capillary vessels, we still could evaluate glomerular filtration indirectly [Fig. 2(b)]. FD 10 kDa flowed into the capillary blood vessels and proximal tubules at the same time, which indicate that FD 10 kDa were immediately filtered by glomerulus. FD 10 kDa flowed into the distal tubules shortly afterward, until all the tubules were filled. The albumin - Evan's blue dye complex remained in blood circulation throughout the study for 60 minutes. Observation of the albumin - Evan's blue dye complex also depicted tumor vasculature [Fig. 3(a)]. Multiple frames were merged to produce a wide-area image [Fig. 3(b)].

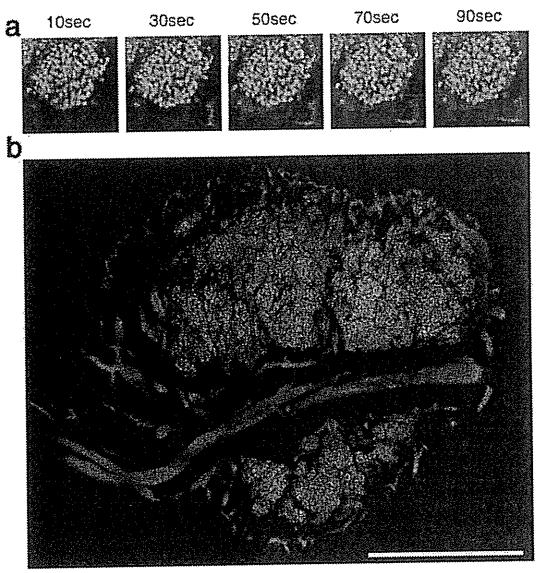

Fig. 3. (a) Intravital confocal micro-videography of subcutaneous HeLa-H2BGFP tumor. Evan's blue dye was administered via tail vein catheter 10 seconds after movie acquisition was initiated. Image frames were extracted from the video at indicated time points. Image size: 212.13μm x 212.13μm (b) Motorized XY stage enables 'large image acquisition' feature of the Nikon NIS-Elements C software. Multiple frames were automatically captured in sequence and merged to produce a wide-area image. Scale bar: 1 mm.

Arterial entrance, venous migration, extravasation into tissue, and clearance was directly observed within various tissues and organs. The intravital confocal micro-videography technique described here is useful for investigating biological mechanisms and functions in both spatial and temporal resolution. Our technique is particularly effective for investigating the dynamic and complex events that occur immediately following drug administration, such as first path effects, site-specific drug accumulation, blood circulation and metabolism behavior.

Materials and methods

Microscope

All picture/movie acquisitions were performed using a Nikon A1R confocal laser scanning microscope system attached to an upright ECLIPSE FN1 (Nikon Corp., Tokyo, Japan). The A1R incorporates both conventional a galvano scanner and also a high-speed resonant scanner. The resonant scanner allows an acquisition speed of 30 frames per second while

#135496 - $15.00 USD Received 27 Sep 2010; revised 16 Oct 2010; accepted 17 Oct 2010; published 21 Oct 2010

maintaining high resolution of 512 × 512 scanned points. Modification of the ECLIPSE FN1 was necessary for intravital imaging because this upright microscope is originally designed for imaging thin, sectioned slices, and not for live animals. The trans-illumination unit (halogen lamp, condenser, sub-stage and turret) was removed entirely from the microscope, as confocal imaging never requires transmitted light, which allowed for more space between the microscope stage and the objective lens. The motorized stage was set as low as possible onto a customized framework, and a custom-designed height-adjustable mouse stage was fixed onto the motorized stage. Small temperature controller (Thermoplate; Tokai Hit Co., Ltd., Shizuoka, Japan) was integrated to the mouse stage [Fig. 1(a)]. For sample imaging, a custom-designed height adjustable coverslip holder is placed onto the tissue of interest to provide a flat surface for the objective lens [Fig. 1(b)]. The coverslip must be perpendicular to the objective lens, tightly fixed, and rigid enough so that the tissue of interest will not move during the imaging, but not so tight as to restrict blood flow. The detailed blueprint of the custom-designed mouse stage and the coverslip holder (fabricated and assembled by Sigma Koki Co. Ltd., Tokyo, Japan) will be provided upon request.

Fluorescent reagents

Hoechst 33342 dye (8 mg/kg in PBS, Lonza Group Ltd., Basel, Switzerland) was used to stain the nuclei of cells present in circulation and in the perivascular space. Evans Blue dye (8 mg/kg in PBS, Wako Pure Chemical Industries, Ltd., Osaka, Japan), which binds to plasma albumin, was used to stain the vasculature. Fluorescein (4 mg/kg in PBS, molecular weight of 332.31, Alcom Japan, Ltd., Tokyo, Japan) and fluorescein-labeled dextrans with average molecular weights of 10k, 70k, 500k (Invitrogen Corporation, Carlsbad, CA, USA) were used to study molecular weight-dependent pharmacokinetics. For the comparison study of normal and hyrodynamic injection, psFLT-1 plasmid DNA was labeled with Cy5 using Label IT Tracker Nucleic Acid Localization Kits (Mirus Bio Corporation, Madison, WI, USA).

Surgical procedures

All animal experimental procedures were executed in accordance with the Guide for the Care and Use of Laboratory Animals as stated by the National Institutes of Health. Mice were anesthetized with 2.0-3.0% isoflurane (Abbott Japan Co., Ltd., Tokyo, Japan) using a Univenter 400 Anaesthesia Unit (Univentor Ltd., Zejtun, Malta). Mice were then subjected to lateral tail vein catheterization with a 30-gauge needle (Becton, Dickinson and Co, Franklin Lakes, NJ, USA) connected to a non-toxic, medical grade polyethylene tube (Natsume Seisakusho Co., Ltd., Tokyo, Japan). Catheterization technique is described elsewhere (http://imaging.bme.ucdavis.edu/surgical.html). This catheterization allows multiple and timed injection without moving the mouse during data acquisition.

Ear lobe dermis tissue was accessible without surgery and easily fixed beneath the cover slip with a single drop of immersion oil. Tumor, kidney, or liver tissues were accessed following exteriorization through skin incision. For tumor imaging, female BALB/c nude mice were inoculated subcutaneously with H2B-GFP cells, which express green fluorescence protein in cell nuclei. Tumors were allowed to mature until the size of the tumor reached 5 mm in diameter. To minimize bleeding during the surgical procedure required to present tumors for imaging, a Surgitron (R) radio-frequency surgical device equipped with a Vari-Tip (TM) Wire Electrode (Cat. No. A8D) (Ellman International Inc., Oceanside, NY, USA) was used for bloodless, micro smooth incision with minimal tissue alteration.

Movie and time-lapse image acquisition

Video acquisition at a speed of 30 frames per second was performed for the indicated times, followed by time-lapse imaging every 1 minute. Drugs were administered via the tail vein catheter 10 seconds after video acquisition was initiated.

#135496 - $15.00 USD Received 27 Sep 2010; revised 16 Oct 2010; accepted 17 Oct 2010; published 21 Oct 2010

Acknowledgments

We thank Teru Kanda (Aichi Cancer Center Research Institute) for HeLa H2B-GFP cells. We thank Masabumi Shibuya (Tokyo Medical and Dental University) for providing pVL 1393 baculovirus vector pDNA encoding human sFLT-1. We thank Yoko Hasegawa, Mika Zenibayashi, Kotoe Date, Satomi Ogura, and Katsue Morii (The University of Tokyo) for technical assistance. T.O. is an employee of Nikon Instech Co., Ltd. All other authors declare no conflict of interest. This work was supported by Core Research Program for Evolutional Science and Technology (CREST) from the Japan Science and Technology Corporation (JST) (K.K.), Funding Program for World-Leading Innovative R&D on Science and Technology (FIRST Program) from Japan Society for the Promotion of Science (JSPS)(K.K.), and Grants-in-Aid for Scientific Research from the Japanese Ministry of Education, Culture, Sports, Science and Technology of Japan (21890051) (Y.M.).

#135496 - $15.00 USD Received 27 Sep 2010; revised 16 Oct 2010; accepted 17 Oct 2010; published 21 Oct 2010

Acta Oto-Laryngologica, 2010; 130: 101–104

informa
healthcare

ORIGINAL ARTICLE

Inner ear drug delivery system from the clinical point of view

TATSUNORI SAKAMOTO[1], TAKAYUKI NAKAGAWA[1], RIE T. HORIE[1], HARUKAZU HIRAUMI[1], NORIO YAMAMOTO[1], YAYOI S. KIKKAWA[2] & JUICHI ITO[1]

[1]*Department of Otolaryngology, Head and Neck Surgery, Graduate School of Medicine, Kyoto University, Kyoto and* [2]*Department of Otolaryngology, Faculty of Medicine, University of Tokyo, Tokyo, Japan*

Abstract

Conclusion: Three types of inner ear drug delivery systems (DDS) that were ready to be applied in clinics were developed. *Objectives:* To develop clinically applicable inner ear DDS for the treatment of inner ear disorders. *Methods:* Inner ear DDS using clinically applicable materials were developed and evaluated. *Results:* The systemic application of stealth-type nanoparticles encapsulating betamethasone provided superior therapeutic results for the treatment of noise-induced hearing loss compared with the systemic application of betamethasone in mice. Microparticles made of biodegradable polymer (poly (lactic/glycolic) acid, PLGA) encapsulating lidocaine were placed on the round window membrane of guinea pigs, and resulted in reasonable concentrations of lidocaine in the cochlea without serious adverse effects. The phase I/IIa clinical trial of the application of insulin-like growth factor-1 (IGF-1) in combination with gelatin hydrogel on the round window membrane was conducted, recruiting patients with acute sensorineural hearing loss after the failure of systemic application of steroids.

Keywords: *Sensorineural hearing loss, tinnitus, biodegradable polymer, gelatin hydrogel, betamethasone, insulin-like growth factor 1, lidocaine*

Introduction

Sensitive sensors in the inner ear, hair cells, are mechanically protected in the bony capsule. The unique high potassium environment required for hair cells to work is actively maintained in the endolymph, which is sealed by tight junctions. The blood–labyrinthine barrier [1] is partly composed of tight junctions and also a system to protect these delicate cells from agents that may cause damage. However, these isolation systems make inner ear diseases difficult to be treated. Direct access into the inner ear is difficult because of the bony capsule. The blood flow of the inner ear is accordingly limited; 1/10 000 of cardiac output in rodents and 1/1 000 000 in humans [2]. It is difficult to deliver systemically applied therapeutic agents into the inner ear because of this limited blood flow and the existence of the blood–labyrinthine barrier [3]. Specific strategies to deliver therapeutic agents into the inner ear are required to overcome this difficulty.

The purpose of a drug delivery system (DDS) is to deliver a drug to a specific site in a specific time and release pattern [4]. Several types of inner ear-specific DDS have been developed, most of which use the round window (RW) as a route to deliver the agent into the inner ear, because the RW is a unique structure in that the inner ear is not covered with bone but sealed with a RW membrane (RWM). One well studied example of inner ear DDS is RWμCath™ (DURECT™ Co., Cupertino, USA), which utilizes the catheter tip placed on the RWM to deliver the therapeutic agent. Plontke et al. [5] conducted a clinical trial using this device. Patients with acute

Correspondence: Tatsunori Sakamoto, 54 Shogoin Kawara-cho, Sakyo-ku, Kyoto 606-8507, Japan. Tel: +81 75 751 3346. Fax: +81 75 751 7225. E-mail: sakamoto@ent.kuhp.kyoto-u.ac.jp

(Received 1 April 2010; accepted 14 April 2010)

ISSN 0001-6489 print/ISSN 1651-2251 online © 2010 Informa Healthcare
DOI: 10.3109/00016489.2010.486801

sensorineural hearing loss and insufficient recovery after systemic glucocorticoid treatment were included in that study, and significantly better improvement of hearing after a continuous intratympanic delivery of glucocorticoid via RWμCath was observed. This device would be applicable to other therapeutic agents; however, major surgery is required before and after the drug application, and more seriously, it is impossible to use this device because this has been commercially discontinued.

It is obviously mandatory to develop clinically applicable and available inner ear DDS. Here we show our approaches to realize this aim. The first is the systemic approach to deliver drugs to the inner ear more effectively. The other two involve local drug delivery via the RWM.

Material and methods

Inner ear DDS via systemic application – stealth-type nanoparticles

It would be more useful and its clinical application would be wider if a systemically applied therapeutic agent could be delivered selectively into the inner ear; however, to date, there is no reported system available to achieve this aim. Instead, we tried to improve the utilization of drugs in the inner ear. We used stealth-type nanoparticles for this purpose, which are made of biodegradable polymer, poly lactic acid (PLA), with polyethylene glycol coating (Figure 1A). Stealth-Nano-Steroid, stealth-type nanoparticles containing betamethasone, have been shown to accumulate preferentially in artificially inflamed joints as a model of rheumatoid arthritis and to reduce inflammation [6]. We first tested the distribution of stealth-type nanoparticles in the inner ear. In terms of clinical application, PLA is widely used as absorbable surgical threads, pins, screws and facial injectables (Sculptra®). Also, polyethylene glycol (PEG) is frequently used to modify the molecular weight, size and solubility of therapeutic drugs. These factors support the clinical safety of Stealth-Nano-Steroid.

Inner ear drug delivery via the round window

Intratympanic injection has been used as a method to realize inner ear treatment to deliver aminoglycosides, steroids and other therapeutic drugs [7]. However, the pharmacokinetics of intratympanically applied drugs are not stable because of the dynamic environment of the tympanic cavity; e.g. liquid in the tympanic cavity is easily ejected into pharynx by swallowing. To stabilize drug delivery via the RWM into the inner ear, we used microparticles made of biodegradable polymer and gelatin hydrogel. These slow releasing materials are placed on the RWM, and as these degrade, encapsulated therapeutic molecules diffuse into the inner ear.

Local application using PLGA microparticles

While tinnitus is a common symptom among patients with hearing impairment, no specific therapeutic strategy has been established. Lidocaine is known to be effective via intratympanic application [8,9]. However, it has been an unacceptable option because of its short effective duration (up to several hours) and serious vertigo after the application due to inner ear anesthesia [10]. We designed the inner ear DDS to reduce the concentration in the inner ear and elongate the release of lidocaine [11]. Poly (lactic/glycolic) acid (PLGA) is another commonly used biodegradable polymer. PLGA microparticles encapsulating lidocaine (Figure 1B) were applied on the RWM of guinea pigs and the lidocaine concentrations in the cochlea were measured at various time points.

Local application using gelatin hydrogels

Gelatin is a natural polymer composed mainly of collagen. By crosslinking with glutaraldehyde, gelatin forms hydrogel. The isoelectric point of gelatin can be modified to yield either a negatively charged acidic gelatin or a positively charged basic gelatin at physiological pH. This allows specific design so that electrostatic interaction takes place between a charged bioactive molecule (e.g. proteins and plasmid DNAs) and gelatin. The crosslinking density of gelatin hydrogels affects their degradation rate. Accordingly, gelatin hydrogels can be used as a delivery vehicle for the controlled release of bioactive molecules [12] (Figure 1C).

Various growth factors including brain-derived neurotrophic factor (BDNF) [13], hepatocyte growth factor (HGF) [14] and insulin-like growth factor 1 (IGF-1) have been placed on the RWM of the cochlea in combination with gelatin hydrogel to test the possibility of their use as therapeutic agents for the treatment of hearing impairment in rodents. Among them, IGF-1 has been shown to be protective [15] and therapeutic [16] against noise-induced inner ear damage, and therapeutic against ischaemic inner ear damage [17]. In addition, recombinant human IGF-1 (rhIGF-1, Mecasermin®, Astellas Pharma Inc., Tokyo, Japan) is commercially available as an orphan drug for

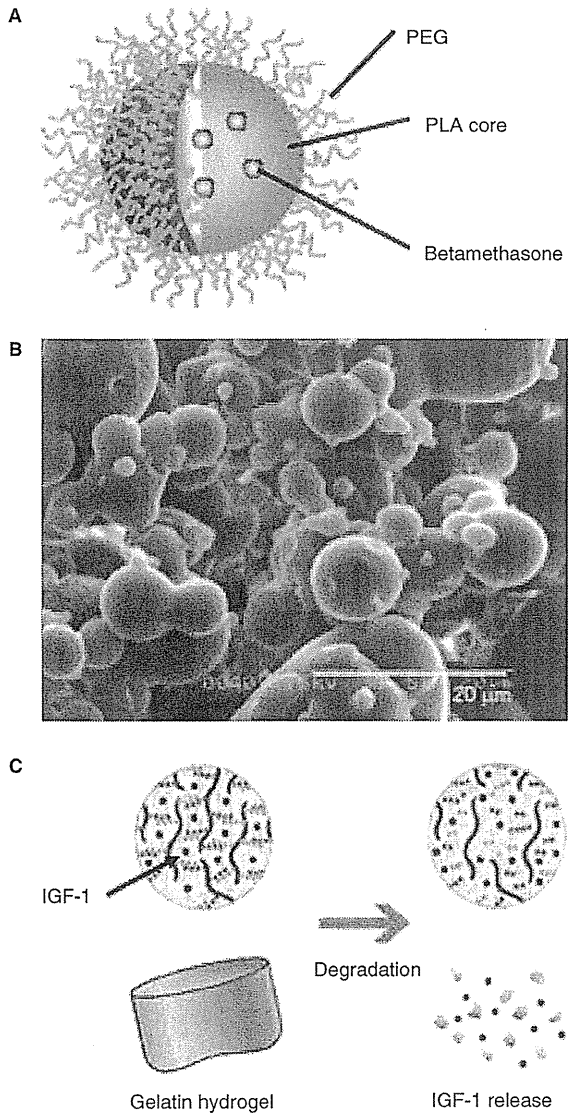

Figure 1. (A) Schematic illustration of a stealth-type poly lactic acid (PLA) nanoparticle with polyethylene glycol (PEG) coating and encapsulated betamethasone. (B) Scanning electron microscopic view of poly (lactic/glycolic) acid (PLGA) microparticles encapsulating lidocaine. (C) Schematic illustration of a gelatin hydrogel drug delivery system (DDS). Target molecules (IGF-1) entrapped in the crosslinked gelatin polymer are gradually released from the polymer matrix as gelatin hydrogel degrades.

the treatment of a type of juvenile growth failure, a certain type of diabetes mellitus and dwarfness.

Against this background, we conducted and have finished a phase I/IIa clinical trial to examine the safety and efficacy of local IGF-1 application via the RWM using gelatin hydrogel for patients with acute sensorineural hearing loss (UMIN000000936). Subjects are patients with acute sensorineural hearing loss, (1) with abnormality in evoked otoacoustic emission, (2) within 29 days after the onset of hearing loss, (3) determined as non-responders to systemic steroid application, and (4) age over 20 years. Major exclusion criteria are (1) presenting active middle ear abnormality, (2) history of previous other treatments including systemic application of batroxobin, prostaglandin I, and hyperbaric oxygen therapy, except for systemic steroid application. Each registered patient received a tympanotomy and the RW niche was inspected with a thin endoscope. Gelatin hydrogel combined with recombinant human IGF-1 (rhIGF-1) was placed on the RWM. Average hearing levels and adverse events were followed up for 24 weeks.

Results and Discussion

Inner ear DDS via systemic application – stealth-type nanoparticles

The systemic application of conventional nanoparticles made of PLGA without PEG coating did not lead to distribution in the inner ear [18]. On the other hand, stealth nanoparticles encapsulating rhodamine B distributed to the inner ear. Systemic application of Stealth-Nano-Steroid after the noise-induced hearing loss showed higher concentrations of betamethasone in the inner ear, and better recovery of hearing compared with the simple systemic application of betamethasone (in print).

Local application using PLGA microparticles

When PLGA microparticles encapsulating lidocaine (Figure 1B) were applied on the RWM of guinea pigs and the lidocaine concentrations in the cochlea were measured at various time points, the highest concentrations were observed on day 3. Nystagmus was not induced by this procedure. Hearing thresholds determined by auditory brainstem responses showed only temporal elevation on day 7. Inflammatory responses in the middle and inner ear were not observed except for minor mucosal thickening and lymphatic cell infiltrations. These results suggest a high possibility for the clinical application of these particles for the treatment of tinnitus without causing serious adverse effects [11]. Animal experiments to show the effectiveness of these particles are difficult because tinnitus is a subjective symptom; however, there are a number of animal models to evaluate tinnitus in rodents [19,20]. We are investigating the effects on the reduction of tinnitus in rodents, and at the same time, a clinical trial is planned.

Local application using gelatin hydrogels

With this method, average hearing levels were comparable to hyperbaric oxygen therapy, which we usually use as a rescue after the failure of systemic steroid therapy. No serious related adverse events were observed. Details of the results will be published separately.

Conclusions

We have developed several DDS that can be used for the treatment of inner ear diseases. All the materials described above were selected from those that are already used in clinics to facilitate clinical applications. These strategies will become templates to realize clinical application of other candidate agents for the treatment of inner ear diseases. We would like to focus more on the demonstration of clinical usefulness of these inner ear DDS.

Acknowledgments

This study was supported by Grant-in-Aids for Researches from the Japanese Ministry of Health, Labour and Welfare and from the the Ministry of Education, Culture, Sports, Science and Technology. Stealth-type nanoparticles were kindly provided by Dr Tsutomu Ishihara (Research Institute for Drug Discovery, Graduate School of Medical Sciences, Kumamoto University) and Prof. Megumu Higaki (Jikei University School of Medicine). Microparticles encapsulating lidocaine and the IGF-1 releasing system using gelatin hydrogel were developed with the intensive support of Prof. Yasuhiko Tabata (Department of Biomaterials, Institute for Frontier Medical Sciences, Kyoto University). The clinical trial was totally supported by Prof. Ken-ichi Inui (Department of Pharmacy, Kyoto University Hospital) and the Translational Research Center of Kyoto University Hospital.

Declaration of interest: The authors report no conflicts of interest. The authors alone are responsible for the content and writing of the paper.

References

[1] Shulman A, Goldstein B. Brain and inner-ear fluid homeostasis, cochleovestibular-type tinnitus, and secondary endolymphatic hydrops. Int Tinnitus J 2006;12:75–81.

[2] Nakashima T, Naganawa S, Sone M, Tominaga M, Hayashi H, Yamamoto H, et al. Disorders of cochlear blood flow. Brain Res Brain Res Rev 2003;43:17–28.

[3] Juhn SK, Hunter BA, Odland RM. Blood-labyrinth barrier and fluid dynamics of the inner ear. Int Tinnitus J 2001;7:72–83.

[4] Simó C, Cifuentes A, Gallardo A. Drug delivery systems: polymers and drugs monitored by capillary electromigration methods. J Chromatogr B Analyt Technol Biomed Life Sci 2003;797:37–49.

[5] Plontke S, Löwenheim H, Preyer S, Leins P, Dietz K, Koitschev A, et al. Outcomes research analysis of continuous intratympanic glucocorticoid delivery in patients with acute severe to profound hearing loss: basis for planning randomized controlled trials. Acta Otolaryngol 2005;125:830–9.

[6] Ishihara T, Kubota T, Choi T, Higaki M. Treatment of experimental arthritis with stealth-type polymeric nanoparticles encapsulating betamethasone phosphate. J Pharmacol Exp Ther 2009;329:412–17.

[7] Salt AN, Plontke SKR. Local inner-ear drug delivery and pharmacokinetics. Drug Discov Today 2005;10:1299–306.

[8] Podoshin L, Fradis M, David YB. Treatment of tinnitus by intratympanic instillation of lignocaine (lidocaine) 2 per cent through ventilation tubes. J Laryngol Otol 1992;106:603–6.

[9] Sakata H, Kojima Y, Koyama S, Furuya N, Sakata E. Treatment of cochlear tinnitus with transtympanic infusion of 4% lidocaine into the tympanic cavity. Int Tinnitus J 2001;7:46–50.

[10] Adunka O, Moustaklis E, Weber A, May A, von Ilberg C, Gstoettner W, et al. Labyrinth anesthesia – a forgotten but practical treatment option in Ménière's disease. ORL J Otorhinolaryngol Relat Spec 2003;65:84–90.

[11] Horie RT, Sakamoto T, Nakagawa T, Tabata Y, Okamura N, Tomiyama N, et al. Sustained delivery of lidocaine into the cochlea using poly lactic/glycolic acid microparticles. Laryngoscope 2010;120:377–83.

[12] Young S, Wong M, Tabata Y, Mikos AG. Gelatin as a delivery vehicle for the controlled release of bioactive molecules. J Control Release 2005;109:256–74.

[13] Endo T, Nakagawa T, Kita T, Iguchi F, Kim T-S, Tamura T, et al. Novel strategy for treatment of inner ears using a biodegradable gel. Laryngoscope 2005;115:2016–20.

[14] Inaoka T, Nakagawa T, Kikkawa YS, Tabata Y, Ono K, Yoshida M, et al. Local application of hepatocyte growth factor using gelatin hydrogels attenuates noise-induced hearing loss in guinea pigs. Acta Otolaryngol 2009;129:453–7.

[15] Iwai K, Nakagawa T, Endo T, Matsuoka Y, Kita T, Kim T-S, et al. Cochlear protection by local insulin-like growth factor-1 application using biodegradable hydrogel. Laryngoscope 2006;116:529–33.

[16] Lee KY, Nakagawa T, Okano T, Hori R, Ono K, Tabata Y, et al. Novel therapy for hearing loss: delivery of insulin-like growth factor 1 to the cochlea using gelatin hydrogel. Otol Neurotol 2007;28:976–81.

[17] Fujiwara T, Hato N, Nakagawa T, Tabata Y, Yoshida T, Komobuchi H, et al. Insulin-like growth factor 1 treatment via hydrogels rescues cochlear hair cells from ischemic injury. Neuroreport 2008;19:1585–8.

[18] Tamura T, Kita T, Nakagawa T, Endo T, Kim T-S, Ishihara T, et al. Drug delivery to the cochlea using PLGA nanoparticles. Laryngoscope 2005;115:2000–5.

[19] Mahlke C, Wallhäusser-Franke E. Evidence for tinnitus-related plasticity in the auditory and limbic system, demonstrated by arg3.1 and c-fos immunocytochemistry. Hear Res 2004;195:17–34.

[20] Turner JG, Parrish J. Gap detection methods for assessing salicylate-induced tinnitus and hyperacusis in rats. Am J Audiol 2008;17:S185–S192.

Neuroscience Letters 487 (2011) 12–16

Contents lists available at ScienceDirect

Neuroscience Letters

journal homepage: www.elsevier.com/locate/neulet

Hydrogen in drinking water attenuates noise-induced hearing loss in guinea pigs

Ying Lin [a], Akinori Kashio [b], Takashi Sakamoto [b], Keigo Suzukawa [b], Akinobu Kakigi [b], Tatsuya Yamasoba [b,*]

[a] Department of Otolaryngology and Head and Neck Surgery, Xijing Hospital, Xi'an, China
[b] Department of Otolaryngology and Head and Neck Surgery, University of Tokyo, Tokyo, Japan

ARTICLE INFO

Article history:
Received 14 July 2010
Received in revised form
17 September 2010
Accepted 23 September 2010

Keywords:
Temporary threshold shift
Oxidative stress
Cochlea
Hair cell

ABSTRACT

It has been shown that molecular hydrogen acts as a therapeutic and preventive antioxidant by selectively reducing the hydroxyl radical, the most cytotoxic of the reactive oxygen species. In the present study, we tested the hypothesis that acoustic damage in guinea pigs can be attenuated by the consumption of molecular hydrogen. Guinea pigs received normal water or hydrogen-rich water for 14 days before they were exposed to 115 dB SPL 4-kHz octave band noise for 3 h. Animals in each group underwent measurements for auditory brainstem response (ABR) or distortion-product otoacoustic emissions (DPOAEs) before the treatment (baseline) and immediately, 1, 3, 7, and 14 days after noise exposure. The ABR thresholds at 2 and 4 kHz were significantly better on post-noise days 1, 3, and 14 in hydrogen-treated animals when compared to the normal water-treated controls. Compared to the controls, the hydrogen-treated animals showed greater amplitude of DPOAE input/output growth functions during the recovery process, with statistical significance detected on post-noise days 3 and 7. These findings suggest that hydrogen can facilitate the recovery of hair cell function and attenuate noise-induced temporary hearing loss.

Exposure to loud noise may cause sensorineural hearing loss that can last for minutes, hours, days, or permanently, depending on the parameters of the acoustic overstimulation and the subject's susceptibility to noise exposure. Noise-induced temporary threshold shift (TTS) is a reversible elevation in hearing threshold that occurs after acoustic overstimulation. TTS can be an indicator of exposures that lead to permanent hearing loss after multiple, cumulative exposure events. Although the mechanisms underlying this phenomenon are not fully understood, it is widely accepted that direct mechanical damage and/or indirect metabolic alterations may be involved. Most notably, the generation of reactive oxygen species (ROS) [12], which may serve as triggers for necrosis or apoptosis, results in damage to the cochlear hair cells and the subsequent degeneration of auditory neurons. Thus, suitable antioxidants are desired to protect against oxidative damage in the inner ear. Pharmacological agents effective against TTS may have a potential clinical role in the prophylaxis of acute acoustic damage. However, most antioxidants have difficulty reaching the cochlear hair cells because of the blood–labyrinthine barrier.

Recent studies have revealed that molecular hydrogen mediates beneficial effects in different systems as an optimal antioxidant agent by selectively scavenging free hydroxyl radicals (•OH) [23,25]. Inhaled hydrogen gas can prevent or reduce pathological or biochemical changes in animal models of cerebral infarction [23], neonatal hypoxia ischemia [4], hepatic injury [9], intestinal ischemia injury [2], myocardial ischemia-reperfusion injury [11], cisplatin-induced nephrotoxicity [19], polymicrobial sepsis [26], and generalized inflammation [27]. Continuous consumption of hydrogen water can also protect against intestinal ischemia [29], neonatal hypoxia-ischemia [3], chronic allograft nephropathy [5] and acute pancreatitis [6]. It has also been shown to reduce atherosclerotic lesions in apolipoprotein E knock-out mice [24], inactivate oxidative stress in the brain of Parkinson disease rodents [7,8], and prevent stress-induced decline in learning and memory caused by chronic physical restraint [18]. Hydrogen-loaded eye drops can also protect the retina from ischemia-reperfusion injury [21]. A clinical study has shown that consuming hydrogen-rich water improves lipid and glucose metabolism in type 2 diabetes patients [14]. Furthermore, hydrogen-saturated culture medium can protect cochlear hair cells against antimycin A-induced oxidative stress *in vitro* [16].

Because of permeability and few side effects of molecular hydrogen, it is considered especially favorable as a component of inner-ear medicine. In the present study, therefore, we tested the

* Corresponding author at: Department of Otolaryngology and Head and Neck Surgery, Faculty of Medicine, University of Tokyo, Hongo 7-3-1, Bunkyo-ku, Tokyo 113-8655, Japan.
E-mail address: tyamasoba-tky@umin.ac.jp (T. Yamasoba).

0304-3940/$ – see front matter © 2010 Elsevier Ireland Ltd. All rights reserved.
doi:10.1016/j.neulet.2010.09.064

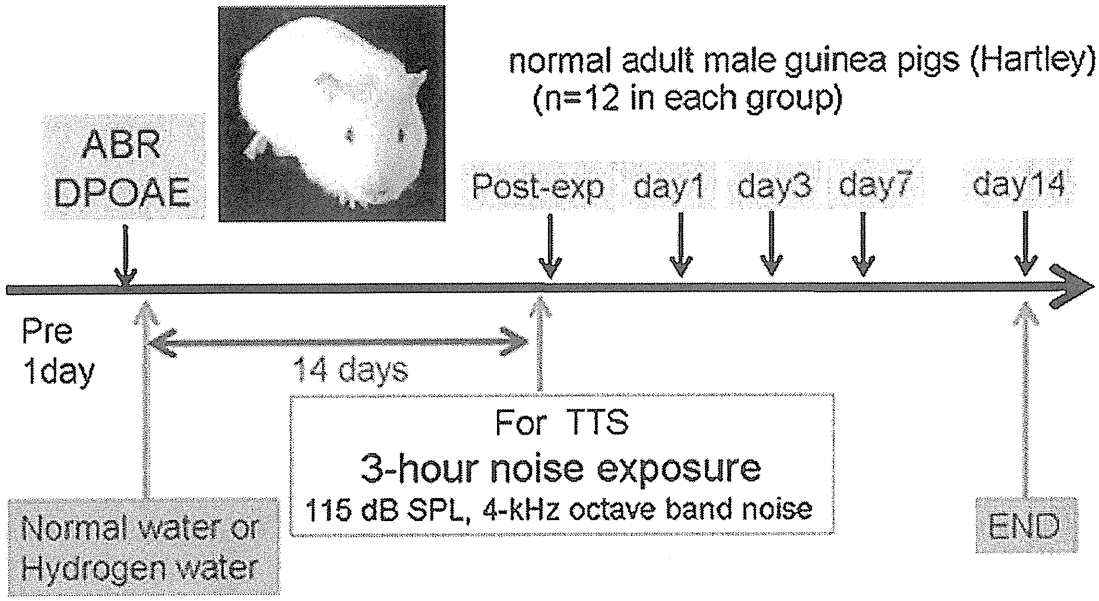

Fig. 1. Schedule of the experiment procedures.

hypothesis that continuous consumption of hydrogen water could attenuate noise-induced TTS in guinea pigs.

Thirty-four male Hartley guinea pigs weighing 250–300 g were used. Since sex differences have been associated with differing ability to detoxify ROS [13], only male guinea pigs were used. One day after arrival, their hearing was confirmed to be within the normal range (within one standard deviation of the normative laboratory baseline) with auditory brainstem response (ABR) or distortion product otoacoustic emissions (DPOAEs) measurements (Fig. 1). After the first baseline hearing tests, animals were randomly divided into normal water-treated and hydrogen water-treated experimental groups ($n = 17$ in each group). Treatment and control solutions were administered orally with unlimited access starting 14 days before noise exposure. Each day, supersaturated hydrogen water (Blue Mercury, Tokyo, Japan) was placed in a closed glass vessel, which minimizes the leakage of hydrogen from the water and maintains the concentration to be greater than 0.4 mM one day later [24]. Weight gains and amounts of water consumed were measured daily. This study was reviewed and approved by the Committee for Ethics in Animal Experiments of the University of Tokyo and carried out under Japanese law and the Guidelines for Animal Experiments of the University of Tokyo.

Fourteen days after starting, either normal or hydrogen water treatments, the animals were subjected to a 3-h noise exposure (115 dB SPL, 4 kHz octave band noise) generated within a single-walled, sound-deadened chamber as previously reported [28]. Two separately caged animals were tested simultaneously and allowed to move freely during exposure. The sound chamber was fitted with speakers driven by a noise generator and power amplifier. A 0.5-in. Bruel and Kjaer condenser microphone and a Fast Fourier Transform analyzer were used to measure and calibrate the sound level at various locations within the chamber to ensure stimulus uniformity within ±1 dB.

To assess the effect of hydrogen water on TTS, 24 animals ($n = 12$ in each group) were subjected to ABR measurements immediately and at 1, 3, 7, and 14 days after noise exposure. The method of ABR measurement has been described previously [15]. In brief, animals were anesthetized intramuscularly with a mixture of xylazine hydrochloride (10 mg/kg) and ketamine hydrochloride (40 mg/kg), and needle electrodes were placed subcutaneously at the vertex (active electrode), beneath the pinna of the measured ear (reference electrode), and beneath the opposite ear (ground). The stimulus duration was 15 ms; the presentation rate, 11/s; the rise/fall time, 1 ms; and the frequencies, 2, 4, 8, and 16 kHz. Responses of 1024 sweeps were averaged at each intensity level. The sound intensity was varied in 5 dB intervals at the intensities close to the threshold, which was defined as the lowest intensity level that produced a clear reproducible waveform peak 3 or 4. In general, amplitude at threshold was approximately 0.1 μV.

Ten animals ($n = 5$ in each group) underwent DPOAE measurement immediately and at 1, 3, 7, and 14 days after noise exposure with an acoustic probe using the DP2000 DPOAE measurement system version 3.0 (Starkey Laboratory, Eden Prairie, MN) as described previously [20]. DP-grams comprised 2f1–f2 DPOAE amplitudes as a function of f2. The stimulus paradigm used for DPOAE input/output (I/O) growth function is constructed as follows [10]: two primary tones with a frequency ratio, f2/f1, of 1.2 were presented, with f2 in one-sixth-octave steps from 1 to 16 kHz. At each frequency pair, primary levels of L2 were incremented in 5 dB steps from 40 to 70 dB SPL with an L1–L2 value of 10 dB. DPOAE was defined to be present when its level exceeded that of the noise floor by 3 dB.

The overall effects of the hydrogen treatment were examined using a two-way factorial analysis of variance with Bonferroni post-tests (SPSS software). p values of less than 0.05 were considered to be statistically significant. Values are expressed as the mean (standard deviation).

Weight gain and the amount of water consumed were not statistically different between the 2 groups (data not shown). Chronological alterations in the ABR threshold shifts at 2, 4, 8, and 16 kHz before and after noise exposure with the application of hydrogen-rich or normal water are shown in Fig. 2. ABR thresholds before noise exposure were essentially equivalent between the 2 groups. In normal water-treated controls, ABR thresholds were moderately increased by approximately 45 dB at all frequencies immediately after noise exposure. Subsequently the ABR thresholds showed gradual recovery, returning to pre-exposure baseline thresholds 14 days later, indicating that the noise exposure induced TTS. Hydrogen-treated animals showed similar but smaller ABR threshold shifts after noise exposure, as compared to the controls.